Pyroelectric and hygrothermal couplings effects on dynamic active control analysis of coupled thermopiezoelastic composite plate

Milad Rouzbehani

Pyroelectric and hygrothermal couplings effects on dynamic active control analysis of coupled thermopiezoelastic composite plate

Milad Rouzbehani

Mechanical Engineering Department,
A. Hashemi Rafsanjani Engineering Campus,
Islamic Azad University of Central Tehran Branch,
Tehran, Iran
Email: roozbehani.milad@gmail.com

Abstract: The main goal of this article is to examine the pyroelectric and hygrothermal couplings effects on dynamic active control analysis of coupled thermopiezoelastic composite plate. The dynamic deflection and stresses of coupled thermopiezoelasticity displayed to hot and humid environmental circumstances are obtained using a direct proportional feedback controller. The governing equations are determined utilising the Navier solution method. The results clearly show that by increasing moisture diffusion, the number of stresses and deflections are increased. Consequently, the induced temperature is increased by increasing humidity up to 25%. A change of 5% deflection rise and on average 4% increase of stresses is observed. Furthermore, if the increase of humidity goes to 75% the plate deflection grows by 9% and stresses increase by about 8%. Additionally, by applying appropriate control gain, the deflection damped 62% quicker which causes the heat generated in the plate controlled properly.

Keywords: coupled thermopiezoelasticity, hygrothermal environment; pyroelectric effect; sensor; actuator; Navier solution.

Biographical notes: Milad Rouzbehani is currently working as an R&D Expert in Iran Aircraft Manufacturing Industry Company. He has obtained his MSc in Applied Design Mechanical Engineering from Azad University, Central Tehran Branch and won the title of the best MSc Thesis award of 2018. He has published several international research articles and has been serving as a reviewer in some of the recognised conferences and journals in his field of research and study.

1 Introduction

Pyroelectricity is a section of specific crystals that is generally electrically polarised and includes huge electric ranges. We can regard pyroelectricity as the capacity of particular substances to produce a transient voltage, regardless of them being cooled or heated

(Cinefra et al., 2017; Hwu et al., 2017). Changes in temperature alter the atoms' conditions somewhat in the structure of the crystal. Provided the temperature remains steady, the voltage of pyroelectric continuously vanishes because of leakage current (Cho et al., 2007; Sereir et al., 2015).

Certain crystals and certain ceramics produce bioelectricity when exposed to thermal changes; a phenomenon called the 'pyroelectric' effect. Pyroelectric crystals correspond to ferroelectric crystals that are centrally asymmetric and exhibit a spontaneous polarisation of Ps. Unlike ferroelectrics, the direction Ps cannot be reversed by an electric field, which is usually temperature-dependent. Therefore, thermal expansion changes the size (length) of the dipoles (Benkhedda and Tounsi, 2008; Lo et al., 2020). Polar impurity molecules are usually adsorbed on the crystals to neutralise surface charges. The pyroelectric effect on a crystal under constant temperature conditions is not detectable but can only appear when the crystal heats up, and the Ps changes. Pyroelectric crystals are mainly used in infrared detectors. They can be spectrally sensitised by coating the surface of the crystal probe with a suitable adsorbent (Brischetto and Carrera, 2018; Heidary and Eslami, 2016).

Three properties are related to the effects of polarisation on crystals. Many materials fall into the general category of dielectrics; their properties, and especially their electrical properties, are affected by electric fields; Piezoelectrics are a subset of dielectrics. Piezoelectrics are electrically charged when subjected to mechanical stress (Eslami et al., 2013; Haghgoo et al., 2019). In contrast, piezoelectrics exert mechanical pressures under the action of an electric field. Pyroelectrics are a subset of piezoelectrics. These materials become polarised on their own, thus producing a pure dipole moment. Some pyroelectric materials are also ferroelectric because the application of an electric field can reverse their polarisation. Therefore, ferroelectric materials are both pyro- and piezoelectric. In addition, pyroelectric materials are piezoelectric; But the opposite is not true, meaning that not all piezoelectrics can be pyroelectric (Eslami et al., 1999; Liu et al., 2012).

By raising the multi-layered composite plates in hot and/or humid environmental circumstances, the hygrothermal response of these plates has extensively drawn attention. The stresses and deformation analysis of various plates exposed to heat and moisture content is a topic of interest to many researchers. Many destructive effects are found in such conditions, like thermal spikes, and thermal oxidation, the durability and hardness of composite degrades due to moisture diffusion. The composites' analysis, which consists of layers of multiple materials subjected to mechanical loading and temperature consequences, has been the research interest of several researchers. Hwu et al. (2017) described the composite sandwich plates and cylindrical shells' free vibration. Cinefra et al. (2017) performed analysis on the layered composite plates. They used an advanced kinematic variable model for their study and also derived relations from virtual displacement, solved by utilising Fourier and Fick's law. Robaldo and Carrera (2007) worked on a finite element combination method for analysing thermos elastic multi-layered plates with variable properties. Cho et al. (2007) analysed the stresses using higher-order shear deformation theory in each composite plate layer. Sousa and coworkers (2013) carried out a finite element investigation of the laminate to anticipate its out-of-plane displacements regarding the two probable and permanent configurations that can be achieved following the curing stage.

The structure of laminated composite is deeply influenced by environmental conditions, including temperature and moisture. An unfavourable environmental situation results in reducing mechanical characteristics, such as structures' hardness and durability.

Wang et al. (2010) examined the hygrothermal conditions' impacts over composite plates interlaminar dynamic stresses along with piezoelectric actuators and sensors. Sereir and coworkers (2015) examined the effects of increasing the moisture content on symmetrical layers in a hygrothermal environment. Lo et al. (2020) measured the hygrothermal impacts over multi-layered composite plates utilising the sophisticated technique. The temperature over the hygrothermal performance of unidirectional laminated plates was exhibited in Sereir et al. (2006). They intended to evaluate an estimated design to assess the stress of hygro-thermo-elastic in composite laminated plates throughout moisture desorption, considering the variation of the mechanical characteristics.

Extensive developments for the analysis of thermal stresses and various composite structures generalised thermoelasticity are well described in the previous studies (Brischetto and Carrera, 2018; Babaei et al., 2018). Brischetto and Carrera (2018) investigated the analysis of thermal stresses using a modified theory for composite shells. Furthermore, the study of thermal stresses employing composite plates and shells combined formulation was carried out by Carrera et al. (2013). They formed the governing equations with a combination of their knowledge and virtual displacement source utilising the Fourier and Fick laws. Heidary and Eslami (2004) studied the dynamic examination of the distributed piezo-thermo-elastic composite plate applying the first-order shear deformation method. Reddy (2006) established a comprehensive and updated operation of classical theory and shear deformation plate and shell theories. Likewise, a number of authors presented the basic theory of coupled piezothermoelasticity (Brunner et al., 2015; Liu et al., 2012).

This paper aims to present the dynamic stresses and deflection variations of a coupled thermo-piezo-elastic rectangular composite plate considering the heat equation resulting from rapidly applied mechanical excitations under a hygrothermal environment. The first-order shear deformation theory is employed so as to define the mechanical displacement field. To that end, a hypothetical linear distribution equation of temperature through the thickness is considered to show the temperature of any point of the plate, which is solved as a coupling with other equations. The thermal coupling is shown to have a substantial impact on the functional response analysis. Controlled and uncontrolled deflections are graphically illustrated.

2 Methodology

Think of a rectangular composite plate of thickness h, width b, length a, whose first and last layers are piezoelectric sensor and actuator described by h_s and h_a, in turn, is assumed in Figure 1. The coordinate axis is placed in the plate corner. The first-order shear deformation approach is included to examine. The plates' global coordinate systems X, Y, and Z, based on the displacement field for the mentioned plate, are assumed as equation (1) (Hwu et al., 2017):

$$u(x, y, z, t) = u_0(x, y, t) + z\psi_1(x, y, t) \tag{1}$$

$$v(x, y, z, t) = v_0(x, y, t) + z\psi_2(x, y, t)$$

$$w(x, y, z, t) = w_0(x, y, t)$$

where W_0 implies the transverse displacement and U_0 and V_0 indicate the in-plane displacements at coordinate location (X, Y, Z) on the mid-plane of the plate.

Figure 1   Schematic of a laminated composite plate with integrated piezoelectric actuator and sensor
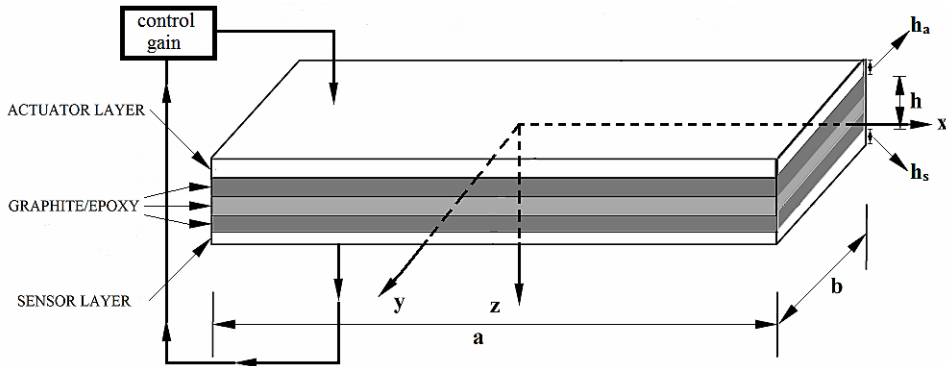
The laminated plate's linear strain-displacement relationship in the material coordinate system implied the equation below (Heidary and Eslami, 2004):

$$\varepsilon_{xx} = \frac{\partial u_0}{\partial x} + z\frac{\partial \psi_1}{\partial x} = \varepsilon_{xx}^0 + z\varepsilon_{xx}^1 \tag{2}$$

$$\varepsilon_{yy} = \frac{\partial v_0}{\partial y} + z\frac{\partial \psi_2}{\partial y} = \varepsilon_{yy}^0 + z\varepsilon_{yy}^1$$

$$\varepsilon_{zz} = 0$$

$$\varepsilon_{yz} = \frac{1}{2}\times\left(\frac{\partial w_0}{\partial y} + \psi_2\right)$$

$$\varepsilon_{xz} = \frac{1}{2}\times\left(\frac{\partial w_0}{\partial x} + \psi_1\right)$$

$$\varepsilon_{xy} = \frac{1}{2}\times\left(\frac{\partial u_0}{\partial y} + z\frac{\partial \psi_1}{\partial y} + \frac{\partial v_0}{\partial x} + z\frac{\partial \psi_2}{\partial x}\right) = \varepsilon_{xy}^0 + z\varepsilon_{xy}^1$$

Equation (2) represents the three-dimensional strain and its connection to generalised mid-plane two-dimensional strains, displayed on the basis of mid-plane displacement gradients. The connection among the two-dimensional displacement field and the three-dimensional generalised displacements is revealed in equation (1).

To correspond the in-plane stress-strain with shear stress-strain relationship, the following constitutive relation of electro-hygro-thermo-elastic formulation with the material coordinate system is mentioned as (Lo et al., 2020):

$$
\begin{Bmatrix} \sigma_{xx} \\ \sigma_{yy} \\ \sigma_{yz} \\ \sigma_{xz} \\ \sigma_{xy} \end{Bmatrix} = \begin{bmatrix} \bar{Q}_{11} & \bar{Q}_{12} & 0 & 0 & \bar{Q}_{16} \\ \bar{Q}_{12} & \bar{Q}_{22} & 0 & 0 & \bar{Q}_{26} \\ 0 & 0 & \bar{Q}_{44} & \bar{Q}_{45} & 0 \\ 0 & 0 & \bar{Q}_{45} & \bar{Q}_{55} & 0 \\ \bar{Q}_{16} & \bar{Q}_{26} & 0 & 0 & \bar{Q}_{66} \end{bmatrix} \left(\begin{Bmatrix} \varepsilon_{xx} \\ \varepsilon_{yy} \\ \varepsilon_{yz} \\ \varepsilon_{xz} \\ \varepsilon_{xy} \end{Bmatrix} - \begin{Bmatrix} \varepsilon_{xx} \\ \varepsilon_{yy} \\ \varepsilon_{yz} \\ \varepsilon_{xz} \\ \varepsilon_{xy} \end{Bmatrix}^{HT} \right) - \begin{bmatrix} 0 & 0 & \bar{e}_{31} \\ 0 & 0 & \bar{e}_{32} \\ 0 & 0 & 0 \\ 0 & 0 & \bar{e}_{35} \\ 0 & 0 & 0 \end{bmatrix} \begin{Bmatrix} E_x \\ E_y \\ E_z \end{Bmatrix} \quad (3)
$$

In equation (3), $\{\sigma\}$ represents the vector of stress, $\bar{Q}_{ij}\{\varepsilon\}$ represents the strain vector because of mechanical loading, [] is the converted constitutive stiffness matrix, $\{\varepsilon\}^{HT}$ represents the strain vector because of the hygrothermal loading, and $\{E\}$ is the vector of the electric field. In this matter, the vector of hygrothermal strain can be expressed in equation (4) as (Brischetto and Carrera, 2018):

$$
\begin{Bmatrix} \varepsilon_{xx} \\ \varepsilon_{yy} \\ \varepsilon_{yz} \\ \varepsilon_{xz} \\ \varepsilon_{xy} \end{Bmatrix}^{HT} = \begin{Bmatrix} \alpha_1 \\ \alpha_2 \\ \alpha_4 \\ \alpha_5 \\ \alpha_6 \end{Bmatrix} \theta + \begin{Bmatrix} \beta_1 \\ \beta_2 \\ \beta_4 \\ \beta_5 \\ \beta_6 \end{Bmatrix} C \quad (4)
$$

where $\{\beta\}$ is the coefficient of moisture and $\{\alpha\}$ is the coefficient of thermal of laminate. C and θ are the concentration of humidity (in %) and temperature variation in Kelvin. The temperature distribution is assumed through the plate thickness and is time dependent in order to monitor the temperature changes at any point of the plate with specific thickness, and at any point in time:

$$
\theta(z, t) = \theta_0 + z\theta_1(t) \quad (5)
$$

where θ_0 and θ_1 in equation (5) are ambient temperature and temperature change through the time, respectively.

2.1 Hamilton's law

So as to calculate the motion equating of a laminated composite plate, Hamilton's principle is applied, where *dv*, *du* and *dk* are virtual work performed by the outside forces, the virtual strain energy, and virtual kinetic energy in turn. This can be applied to the inelastic and elastic continuum as (Heidary and Eslami, 2005):

$$
\delta u_0 : N_{xx,x} + N_{xy,y} = I_0 \ddot{u}_0 + I_1 \ddot{\psi}_1 \quad (6)
$$

$$
\delta v_0 : N_{xy,x} + N_{yy,y} = I_0 \ddot{v}_0 + I_1 \ddot{\psi}_2
$$

$$
\delta w_0 : Q_{x,x} + Q_{y,y} + q = I_0 \ddot{w}_0
$$

$$
\delta \psi_1 : M_{xx,x} + M_{xy,y} - Q_x = I_1 \ddot{u}_0 + I_2 \ddot{\psi}_1
$$

$$
\delta \psi_2 : M_{xy,x} + M_{yy,y} - Q_y = I_1 \ddot{v}_0 + I_2 \ddot{\psi}_2
$$

In the equation above, Q represents the mechanical loading of the applied surface, and I_0, I_1, and I_2 are the inertia's mass moments. equations (6) represents five second-order nonlinear partial differential equations regarding the five generalised displacements u_0, v_0, w_0, ψ_1, and ψ_2. When the strains and rotations are small, u_0 and v_0 that govern the in-plane stretching are uncoupled from w_0, ψ_1 and ψ_2, which correspond to the bending. The quantities Q_x and Q_y are the transverse shear force resultants in x and y directions, M_{xx}, M_{yy}, and M_{xy} are the moments, N_{xx}, N_{yy}, and N_{yx} are in-plane force resultants, which are defined in equations (7)–(9) as follows (Heidary and Eslami, 2016):

$$\begin{Bmatrix} N_{xx} \\ N_{yy} \\ N_{xy} \end{Bmatrix} = \begin{bmatrix} A_{11} & A_{12} & A_{16} \\ A_{16} & A_{22} & A_{22} \\ A_{11} & A_{26} & A_{66} \end{bmatrix} \begin{Bmatrix} \varepsilon_{xx}^0 \\ \varepsilon_{yy}^0 \\ \varepsilon_{xy}^0 \end{Bmatrix} + \begin{bmatrix} B_{11} & B_{12} & B_{16} \\ B_{12} & B_{22} & B_{22} \\ B_{16} & B_{26} & B_{66} \end{bmatrix} \begin{Bmatrix} \varepsilon_{xx}^1 \\ \varepsilon_{yy}^1 \\ \varepsilon_{xy}^1 \end{Bmatrix} - \begin{Bmatrix} N_{xx} \\ N_{yy} \\ N_{xy} \end{Bmatrix}^{HT} - \begin{Bmatrix} N_{xx} \\ N_{yy} \\ N_{xy} \end{Bmatrix}^E \quad (7)$$

$$\begin{Bmatrix} M_{xx} \\ M_{yy} \\ M_{xy} \end{Bmatrix} = \begin{bmatrix} B_{11} & B_{12} & B_{16} \\ B_{12} & B_{22} & B_{26} \\ B_{16} & B_{26} & B_{66} \end{bmatrix} \begin{Bmatrix} \varepsilon_{xx}^0 \\ \varepsilon_{yy}^0 \\ \varepsilon_{xy}^0 \end{Bmatrix} + \begin{bmatrix} D_{11} & D_{12} & D_{12} \\ D_{12} & D_{22} & D_{26} \\ D_{16} & D_{26} & D_{66} \end{bmatrix} \begin{Bmatrix} \varepsilon_{xx}^1 \\ \varepsilon_{yy}^1 \\ \varepsilon_{xy}^1 \end{Bmatrix}$$
$$- \begin{Bmatrix} M_{xx} \\ M_{yy} \\ M_{xy} \end{Bmatrix}^{HT} - \begin{Bmatrix} M_{xx} \\ M_{yy} \\ M_{xy} \end{Bmatrix}^E \quad (8)$$

$$\begin{Bmatrix} Q_y \\ Q_x \end{Bmatrix} = \begin{bmatrix} S_{44} & S_{45} \\ S_{45} & S_{55} \end{bmatrix} \begin{Bmatrix} \varepsilon_{yz} \\ \varepsilon_{xz} \end{Bmatrix} - \begin{Bmatrix} Q_y \\ Q_x \end{Bmatrix}^{HT} - \begin{Bmatrix} Q_y \\ Q_x \end{Bmatrix}^E \quad (9)$$

where the shear stiffness coefficient of the composite plate S_{ij} is assumed as:

$$\begin{bmatrix} A_{44} & A_{45} \\ A_{45} & A_{55} \end{bmatrix} = K_s \begin{bmatrix} S_{44} & S_{45} \\ S_{45} & S_{55} \end{bmatrix} \quad (10)$$

In equation (10), K_s represents the factor of the shear correction, and its value equals 0.91287 for the assumed plate (Heidary and Eslami, 2005). By substituting the forces and moments of equations (7)–(10) into equation (6), the final form of Hamilton's principle is defined as:

$$\frac{\partial^2 w_0}{\partial x^2}\left(\frac{1}{2}S_{55}\right) + \frac{\partial^2 w_0}{\partial y^2}\left(\frac{1}{2}S_{44}\right) + \frac{\partial \psi_1}{\partial x}\left(\frac{1}{2}S_{55}\right) + \frac{\partial \psi_2}{\partial y}\left(\frac{1}{2}S_{44}\right) + q = I_0\frac{\partial^2 w_0}{\partial t^2} \quad (11)$$

$$\frac{\partial^2 u_0}{\partial x^2}\left(B_{11} + \bar{e}_{31}^2\frac{z^2}{2K_{33}}\right) + \frac{\partial^2 v_0}{\partial x \partial y}\left(B_{12} + \bar{e}_{31}\bar{e}_{32}\frac{z^2}{2K_{33}}\right) + \frac{\partial^2 w_0}{\partial x^2}\left(\bar{e}_{31}\bar{e}_{35}\frac{z^2}{4K_{33}}\right)$$
$$+ \frac{\partial w_0}{\partial x}\left(-\frac{1}{2}S_{55}\right) + \frac{\partial^2 \psi_1}{\partial x^2}\left(D_{11} + \bar{e}_{31}^2\frac{z^2}{2K_{33}}\right) + \frac{\partial \psi_1}{\partial x}\left(\bar{e}_{31}\bar{e}_{35}\frac{z^2}{4K_{33}}\right) + \psi_1\left(-\frac{1}{2}S_{55}\right) \quad (12)$$
$$+ \frac{\partial^2 \psi_2}{\partial x \partial y}\left(D_{12} + \bar{e}_{31}\bar{e}_{32}\frac{z^3}{2K_{33}}\right) + \bar{\lambda}_5 z(\theta_0 + z\theta_1) + \bar{\gamma}_5 zc = I_1\frac{\partial^2 u_0}{\partial t^2} + I_2\frac{\partial^2 \psi_1}{\partial t^2}$$

$$\frac{\partial^2 u_0}{\partial x \partial y}\left(B_{12} + \bar{e}_{31}\bar{e}_{32}\frac{z^2}{2K_{33}}\right) + \frac{\partial^2 v_0}{\partial y^2}\left(B_{22} + \bar{e}_{32}^2\frac{z^2}{2K_{33}}\right) + \frac{\partial^2 w_0}{\partial x \partial y}\left(\bar{e}_{32}\bar{e}_{35}\frac{z^2}{4K_{33}}\right)$$

$$+ \frac{\partial w_0}{\partial y}\left(-\frac{1}{2}S_{44}\right) + \frac{\partial^2 \psi_1}{\partial x \partial y}\left(D_{12} + \bar{e}_{31}\bar{e}_{32}\frac{z^2}{2K_{33}}\right) + \frac{\partial \psi_1}{\partial y}\left(\bar{e}_{32}\bar{e}_{35}\frac{z^2}{4K_{33}}\right)$$

$$+ \frac{\partial \psi_2}{\partial y}\left(D_{22} + \bar{e}_{32}^2\frac{z^3}{2K_{33}}\right) + \psi_2\left(-\frac{1}{2}S_{44}\right) + \bar{\lambda}_4 z(\theta_0 + z\theta_1) + \bar{\gamma}_4 zc \tag{13}$$

$$= I_1\frac{\partial^2 v_0}{\partial t^2} + I_2\frac{\partial^2 \psi_2}{\partial t^2}$$

In equations (11)–(13), the components of $\bar{\lambda}$ and $\bar{\gamma}$ are the changed stress-temperature and the coefficients of stress-moisture, respectively.

$$(\bar{\lambda}) = [\bar{Q}](\bar{\alpha}) \tag{14}$$

$$(\bar{\gamma}) = [\bar{Q}](\bar{\beta})$$

2.2 Actuator equations

The layers of piezoelectric function as distributed sensors, as well as actuators, in order to observe and check the structure's dynamic response. The applied electrical field impact over stresses is similar to the temperature field impact. The elements $\{D_i\}$ of the electrical displacement vector are linked to strains and electrical field elements. Hence, the modified equations can be defined (Liew et al., 2015):

$$\begin{Bmatrix} D_x \\ D_y \\ D_z \end{Bmatrix} = \begin{bmatrix} 0 & 0 & 0 & 0 & 0 \\ 0 & 0 & 0 & 0 & 0 \\ \bar{e}_{31} & \bar{e}_{32} & 0 & \bar{e}_{35} & 0 \end{bmatrix}\begin{Bmatrix} \varepsilon_{xx} \\ \varepsilon_{yy} \\ \varepsilon_{yz} \\ \varepsilon_{xz} \\ \varepsilon_{xy} \end{Bmatrix} + \begin{bmatrix} K_{11} & 0 & 0 \\ 0 & K_{22} & 0 \\ 0 & 0 & K_{33} \end{bmatrix}\begin{Bmatrix} E_x \\ E_y \\ E_z \end{Bmatrix} + \begin{Bmatrix} 0 \\ 0 \\ P_3 \end{Bmatrix}\theta \tag{15}$$

where $\{E_i\}$ in equation (15) is the electric field vector, $[\bar{e}_{ij}]$ is the transformed piezoelectric stress coefficient matrix, $[k]$ is the constant value of dielectric, and finally, P_3 represents the pyroelectric constant. This electro-thermo-mechanical equation presents the outset point for the sensor and actuator equations' derivation. Based on the Figure 1, a distributed sensing theory on the basis of the straight piezoelectric impact and the plate strains and temperature are increased. Given the Gauss law, the closed-circuit charge assessed by the kth layer electrodes in the direction Z can be displayed as (Lam et al., 1997):

$$Q_s = \frac{1}{2}\left[\int_{SI(z=z_{k+1})} D_z ds + \int_{SI(z=z_k)} D_z ds\right] \tag{16}$$

$$= \frac{1}{2}a \cdot b\left(\bar{e}_{31}\varepsilon_{xx} + \bar{e}_{32}\varepsilon_{yy} + \bar{e}_{35}\varepsilon_{xz} + K_{33}E_z + P_3(\theta_0 + z\theta_1)\right)$$

By replacement of equations (16) into equation (15), the electric field along the sensor's Z direction can be obtained as:

$$E_z = -\frac{V_s}{h_s}$$

$$= \frac{\bar{e}_{31}\left(\frac{\partial u_0}{\partial x} + z\frac{\partial \psi_1}{\partial x}\right) + \bar{e}_{32}\left(\frac{\partial v_0}{\partial y} + z\frac{\partial \psi_2}{\partial y}\right) + \frac{1}{2}\bar{e}_{35}\left(\frac{\partial w_0}{\partial x} + \psi_1\right) + p_3\left(\theta_0 + z\theta_1\right)}{-K_{33}} \quad (17)$$

where V_s in equation (17) is the voltage of the sensor layer. The converse piezoelectric approach impact is applied to prevent the composite vibration. The actuating voltage V_a under a fixed gain control algorithm is displayed as:

$$V_a = G_a V_s = \frac{G_a h_s \left(\begin{array}{c} \left(\bar{e}_{31}\left(\frac{\partial u_0}{\partial x} + z\frac{\partial \psi_1}{\partial x}\right) + \bar{e}_{32}\left(\frac{\partial v_0}{\partial y} + z\frac{\partial \psi_2}{\partial y}\right)\right) \\ +\frac{1}{2}\bar{e}_{35}\left(\frac{\partial w_0}{\partial x} + \psi_1\right) + p_3\left(\theta_0 + z\theta_1\right) \end{array} \right)}{K_{33}} \quad (18)$$

where G_a in equation (18) represents the supply feedback control gains. The forces and moments of electric actuating can be defined given the sensor layer strain.

2.3   Heat equations

The fundamentals of the entropy equation in the pyroelectric medium with generalised heat theory are addressed. The impact of the applied thermal field and electric field over stresses are comparable. The transformed thermal entropy equation for a coupled thermopiezoelastic composite plate is presented in equation (19) (Heidary and Eslami, 2005):

$$\{\eta\} = \begin{bmatrix} \bar{\lambda}_1 & \bar{\lambda}_2 & \bar{\lambda}_4 & \bar{\lambda}_5 & \bar{\lambda}_6 \end{bmatrix} \begin{Bmatrix} \varepsilon_{xx} \\ \varepsilon_{yy} \\ \varepsilon_{yz} \\ \varepsilon_{xz} \\ \varepsilon_{xy} \end{Bmatrix} + \begin{bmatrix} 0 & 0 & P_3 \end{bmatrix} \begin{Bmatrix} E_x \\ E_y \\ E_z \end{Bmatrix} + \alpha_v \theta \quad (19)$$

In the equation above, η implies the entropy per unit volume and α_v represents the coefficient of thermal expansion described as the material constant, provided by:

$$\alpha_v = \frac{\rho C_v}{\theta} \quad (20)$$

where C_v is the specific heat at fixed volume and ρ represents the material mass density. The thermal field is associated with the heat conduction considering the principle of Fourier as:

$$\{h\} = -[k]\{\nabla\theta\}$$

$$\{\nabla\theta\} = \begin{Bmatrix} \dfrac{\partial\theta}{\partial x} \\ \dfrac{\partial\theta}{\partial y} \\ \dfrac{\partial\theta}{\partial z} \end{Bmatrix} \Rightarrow \{h\} = -\begin{bmatrix} k_x & k_y & k_z \end{bmatrix}\begin{Bmatrix} \dfrac{\partial\theta}{\partial x} \\ \dfrac{\partial\theta}{\partial y} \\ \dfrac{\partial\theta}{\partial z} \end{Bmatrix} \Rightarrow h = -kz\theta_1 \tag{21}$$

$[k]$ in equation (21) represents the heat conduction coefficients matrix, and $\{h\}$ represents the heat conduction flux vector. Considering the generalised heat equation, it can then be formulated as equation (22) (Heidary and Eslami, 2005):

$$\theta_0\dot{\eta} = -\{\nabla\}^T\{h\} \tag{22}$$

Substituting equations (19) to (21) into equation (22) Leads to the heat conduction equation which can be defined as follows:

$$\frac{\partial^2 u_0}{\partial x\partial t}\left(\theta_0\bar{\lambda}_1 - \frac{\theta_0 P_3\bar{e}_{31}}{K_{33}}\right) + \frac{\partial^2 u_0}{\partial y\partial t}\left(\frac{\theta_0\bar{\lambda}_1}{2}\right) + \frac{\partial^2 v_0}{\partial y\partial t}\left(\theta_0\bar{\lambda}_2 - \frac{\theta_0 P_3\bar{e}_{32}}{K_{33}}\right) + \frac{\partial^2 v_0}{\partial x\partial t}\left(\frac{\theta_0\bar{\lambda}_6}{2}\right)$$

$$+ \frac{\partial^2 w_0}{\partial x\partial t}\left(\frac{\theta_0\bar{\lambda}_5}{2} - \frac{\theta_0 P_3\bar{e}_{35}}{2K_{33}}\right) + \frac{\partial^2 w_0}{\partial y\partial t}\left(\frac{\theta_0\bar{\lambda}_4}{2}\right) + \frac{\partial^2\psi_1}{\partial y\partial t}\left(\theta_0\bar{\lambda}_1 - \frac{\theta_0 z P_3\bar{e}_{31}}{K_{33}}\right)$$

$$+ \frac{\partial^2\psi_1}{\partial y\partial t}\left(\frac{\theta_0\bar{\lambda}_6}{2}\right) + \frac{\partial^2\psi_1}{\partial t}\left(\frac{\theta_0\bar{\lambda}_5}{2} - \frac{\theta_0 P_3\bar{e}_{35}}{2K_{33}}\right) + \frac{\partial^2\psi_2}{\partial x\partial t}\left(\frac{\theta_0 z\bar{\lambda}_6}{2}\right) \tag{23}$$

$$+ \frac{\partial^2\psi_2}{\partial y\partial t}\left(\theta_0 z\bar{\lambda}_2 - \frac{\theta_0 z P_3\bar{e}_{32}}{K_{33}}\right) + \frac{\partial\psi_2}{\partial t}\left(\frac{\theta_0\bar{\lambda}_4}{2}\right) + \frac{\partial\theta_1}{\partial t}\left(\theta_0\alpha_v - \frac{\theta_0 P_3^2 z}{K_{33}}\right) = 0$$

3   Results and discussion

A coupled thermo-piezoelectric-mechanical mechanism of the composite laminate plate with surface bonded piezoelectric sensor and actuator subjected to rapidly apply mechanical excitations under a hygrothermal environment is explained in the article. The investigation of a rectangular plate demands solving the governing biharmonic equation, accompanied by proper boundary conditions at the four edges, to yield the deflection function *W*. Once this is carried out, the strains and stresses at any point of the plate structure can be obtained. The basic idea behind Navier's method is to seek the solution for *W* in the form of an infinite series such that the governing differential equation is reduced to simple algebraic equations. Regarding the boundary conditions for the first-order shear deformation plate approach, it can be stated as in equation (24) (Reddy, 2006):

$$w_0(x, 0, t) = w_0(x, b, t) = w_0(0, y, t) = w_0(a, y, t) = 0 \tag{24}$$

$$\psi_1(x, 0, t) = \psi_1(x, b, t) = \psi_2(0, y, t) = \psi_2(a, y, t) = 0$$

$$M_{yy}(x, 0, t) = M_{yy}(x, b, t) = M_{xx}(0, y, t) = M_{xx}(a, y, t) = 0$$

$$\theta(x, 0, t) = \theta(x, b, t) = \theta(0, y, t) = \theta(a, y, t) = \theta_0$$

The boundary conditions in equation (24) are fulfilled by the subsequent displacements expansions:

$$w_0(x, y, t) = \sum_{n=1}^{\infty} \sum_{m=1}^{\infty} W_{mn} \sin \frac{m\pi x}{a} \sin \frac{n\pi y}{b} \tag{25}$$

$$\psi_1(x, y, t) = \sum_{n=1}^{\infty} \sum_{m=1}^{\infty} X_{mn} \cos \frac{m\pi x}{a} \sin \frac{n\pi y}{b}$$

$$\psi_2(x, y, t) = \sum_{n=1}^{\infty} \sum_{m=1}^{\infty} Y_{mn} \sin \frac{m\pi x}{a} \cos \frac{n\pi y}{b}$$

Substitution of equation (25) into equations (11)–(13) and (23) with considering equation (18), yields the next equations for the coefficients (W_{mn}, X_{mn}, Y_{mn}) (Reddy, 2006):

$$
\begin{bmatrix} \hat{S}_{11} & \hat{S}_{12} & \hat{S}_{13} & 0 \\ \hat{S}_{21} & \hat{S}_{22} & \hat{S}_{23} & \hat{S}_{24} \\ \hat{S}_{31} & \hat{S}_{32} & \hat{S}_{33} & \hat{S}_{34} \end{bmatrix}
\begin{Bmatrix} W_{mn} \\ X_{mn} \\ Y_{mn} \\ \theta_{mn} \end{Bmatrix}
+ \begin{bmatrix} \hat{m}_{11} & 0 & 0 & 0 \\ 0 & \hat{m}_{22} & 0 & 0 \\ 0 & 0 & \hat{m}_{33} & 0 \end{bmatrix}
\begin{Bmatrix} \ddot{W}_{mn} \\ \ddot{X}_{mn} \\ \ddot{Y}_{mn} \\ \ddot{\theta}_{mn} \end{Bmatrix}
$$

$$
= \begin{Bmatrix} Q_{mn} \\ 0 \\ 0 \end{Bmatrix} - \begin{Bmatrix} 0 \\ \bar{\lambda}_5 z\theta_0 + \bar{\gamma}_5 zc \\ \bar{\lambda}_4 z\theta_0 + \bar{\gamma}_4 zc \end{Bmatrix} \begin{bmatrix} \hat{n}_{11} & \hat{n}_{12} & \hat{n}_{13} & \hat{n}_{14} \end{bmatrix} \begin{Bmatrix} \dot{W}_{mn} \\ \dot{X}_{mn} \\ \dot{Y}_{mn} \\ \dot{\theta}_{mn} \end{Bmatrix} = 0 \tag{26}
$$

where $[\hat{S}]$, $[\hat{m}]$ and $[\hat{n}]$ in equation (26) are constant-coefficient matrices, and Q_{mn} is the mechanical load. Also W_{mn}, X_{mn}, Y_{mn} and θ_{mn} are coefficients in double Fourier sine series.

For confirmation of the importance of a hygrothermal environment over an intelligent structure, a supported laminated composite plate with dimensions of (90 cm × 90 cm) and both sides surfaces simultaneously bonded by piezoelectric material (as displayed in Figure 1), is investigated. The total thickness is 9 mm. The plate subjects to a quickly applied uniform surface loads of F = 500 N/m². The plate constitutes three composite and two outer piezo layers. The plate consists of a graphite/epoxy layer and two piezoelectric films layers which made of PVDF which material characteristics are provided as shown in Table 1 (Phung-Van et al., 2015).

Table 1 Material characteristics

Property	Graphite/epoxy	PVDF
ρ (kg/m³)	1,578	1,800
E_1 (Gpa)	132.38	2
E_2 (Gpa)	10.76	2
G_{12} (Gpa)	3.61	1
G_{13} (Gpa)	5.65	1
G_{23} (Gpa)	5.65	1
ν_{12}	0.24	0.29
ν_{13}	0.24	0.29
ν_{23}	0.49	0.29
e_{31} (C/m²)	-----	0.046
e_{32} (C/m²)	-----	0.046
e_{35} (C/m²)	-----	0.046
K_{33} (F/m)	-----	0.106×10^{-9}
P_3 (C/m²K)	-----	0.00124
α (1/K)	0.18×10^{-6}	0.9×10^{-6}
β (1/%H₂O)	0.44	0.45
θ_0 (K)	300	300

It is expected that the material characteristics are consistent concerning the change in temperature, and also, the stress and strain relations are linear. For the appropriate evaluation, the dimensionless parameters in equation (27) are used (Ray et al., 2019).

$$\left(\bar{\sigma}_{xz}, \bar{\sigma}_{yz} \right) = \left(\sigma_{xz}, \sigma_{yz} \right)\left(\frac{h}{aq_0} \right), \quad \bar{w} = w_0 \left(\frac{E_2 h^3}{a^4 q_0} \right) \times 10^2$$

$$\left(\bar{\sigma}_x, \bar{\sigma}_y, \bar{\sigma}_{xy} \right) = \left(\sigma_x, \sigma_y, \sigma_{xy} \right)\left(\frac{h^2}{a^2 q_0} \right), \quad \bar{\theta} = \frac{\theta_1}{\theta_0}$$

(27)

Moreover, it is estimated that the simply supported plate's centre is vibrating loosely because of the provided primary surface mechanical load. A specific parametric examination is carried out, concentrating on the remarkable impacts of the hygrothermal environment on the laminated plate. The various dynamic stresses and central deflection with the temperature of the plate are determined in Table 2 based on Navier's method. The outcomes demonstrate that the hygrothermal environment for the different values of the moisture percentage hold a substantial impact over the dynamic stresses and deflection where the σ_{xy} has less effective stresses against σ_x and σ_y Therefore, moisture contents could be considered for improving the optimum design of composite plate under hygrothermal loadings.

Table 2   Numerical results of non-dimensionalised dynamic stresses and deflection

	C = 0%	C = 25%	C = 50%	C = 75%
w	0.4301	0.4533	0.4658	0.4741
σ_x	0.5441	0.5618	0.5732	0.5848
σ_y	0.2009	0.2119	0.2207	0.2253
σ_{xy}	0.0217	0.0221	0.0224	0.0230
σ_{yz}	0.0994	0.1031	0.1063	0.1081
σ_{xz}	0.0986	0.1025	0.1052	0.1076
θ	0.00369	0.00993	0.0121	0.0157

As given by the table data analysis, the moisture change predicts the various deflections. Therefore, for the model under consideration, the central dynamic deflection of the plate has been changed under the hygrothermal environment as shown in Figure 2 with the various moisture contents. It is clear that the increase of moisture causes the enhancement of the deflection. By increasing moisture up to 25%, a change of 5% deflection rise is observed. Besides, due to 50% moisture, the growth of deflection reaches to 8%.

Figure 2   Impact of moisture on the non-dimensionalised dynamic central deflection of the plate
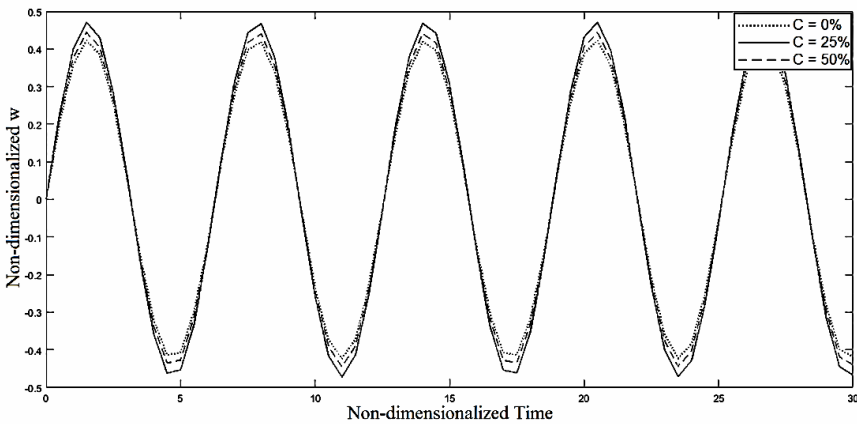
The importance of moisture effect on composite plate stresses with considering the piezoelectric effect is shown in Figures 3 to 7. It demonstrates that the increase of the moisture has the greatest impact on σ_y and the least impact on σ_{xy}. The impact of increasing the moisture on σ_{yz} and σ_{xz} is the same. In 25% moisture, the increase rate of σ_x, σ_y, σ_{xy}, and σ_{xz} reaches 4%, 5%, 2%, and 3%, respectively. Similarly, in 50% moisture, this growth reaches to 5%, 9%, 3% and 6% respectively. So increasing the rate of moisture may lead to destructive effects on the composite plate.

Figure 3 Impact of moisture on non-dimensionalised dynamic normal stress σ_x
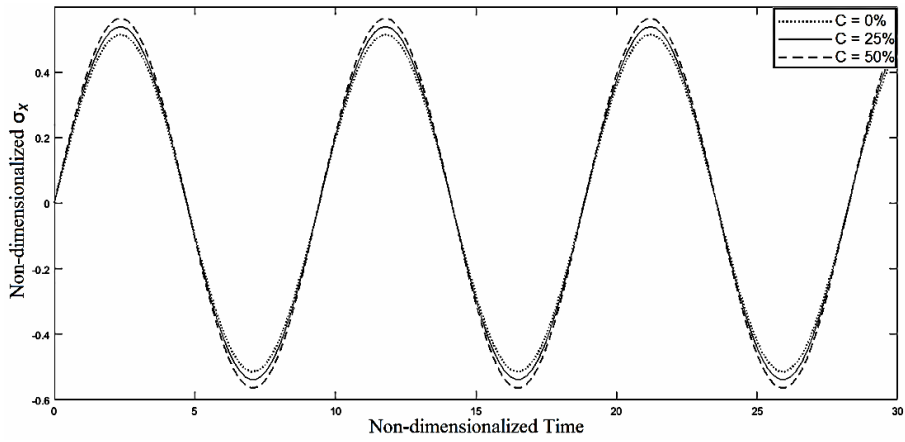
Figure 4 Impact of moisture on non-dimensionalised dynamic normal stress σ_y
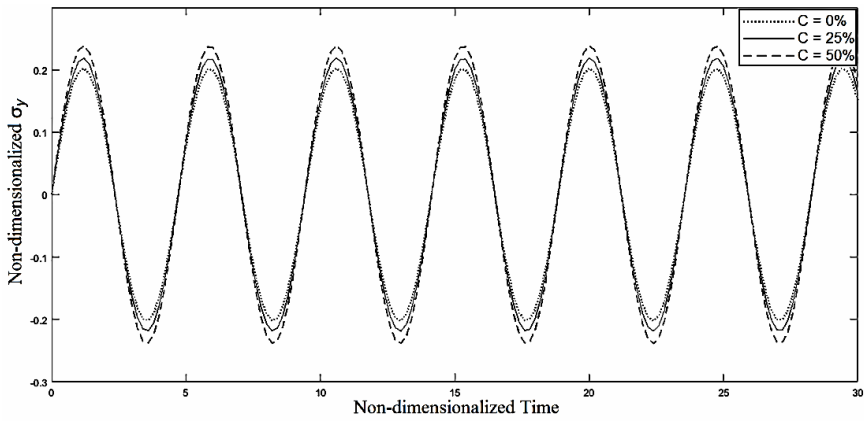
Figure 5 Impact of moisture on non-dimensionalised dynamic shear stress σ_{xy}
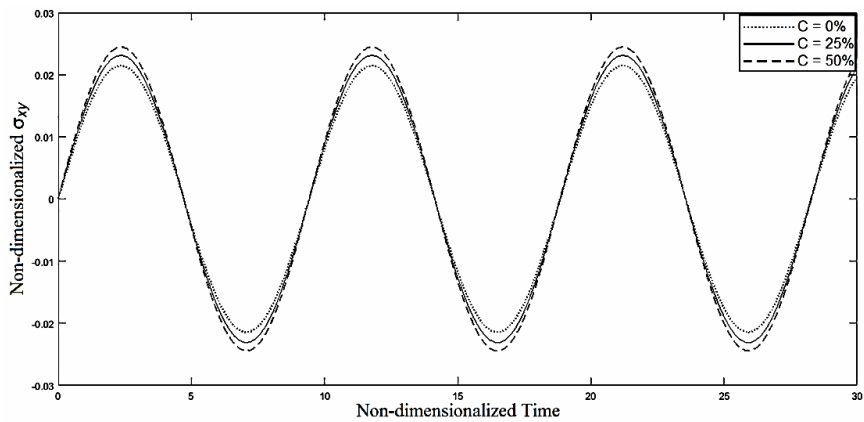
Figure 6   Impact of moisture on non-dimensionalised dynamic shear stress σ_{yz}
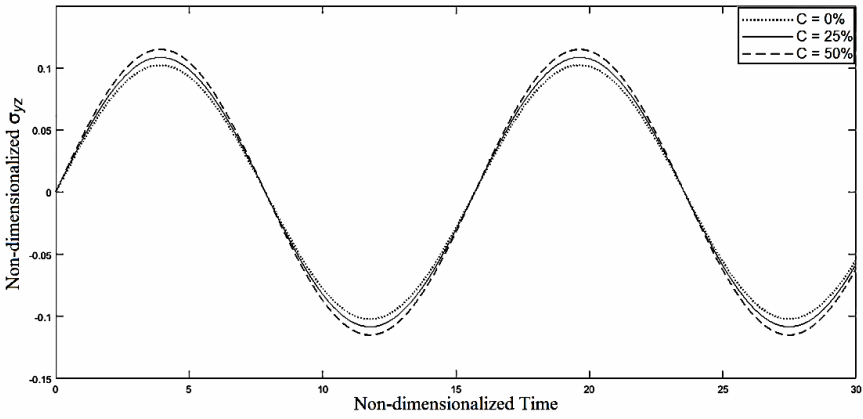
Figure 7   Impact of moisture on non-dimensionalised dynamic shear stress σ_{xz}
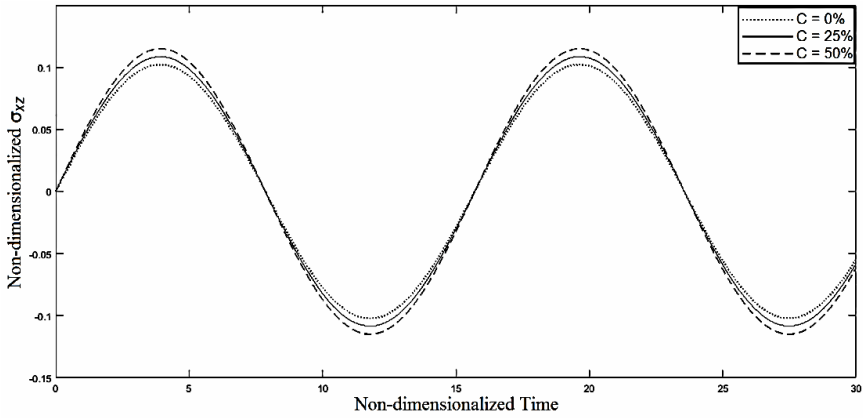
Figure 8   Pyroelectric effect on non-dimensionalised dynamic temperature of the plate
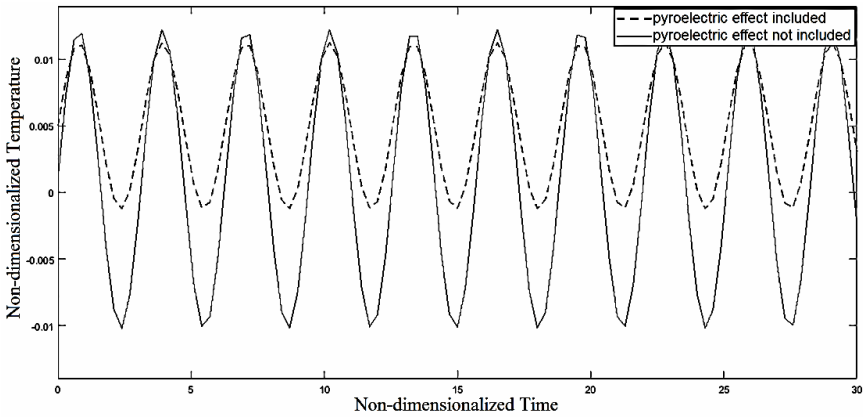
It is interesting to note that the piezoelectric coupling changes the induced temperature in the PVDF layers, which leads to limit the temperature range. This is due to the pyroelectric coefficient being considered for the piezoelectric materials. The significance of the pyroelectric impacts on the temperature range of a composite plate with and without regarding the piezoelectric control impact is presented in Figure 8. Depending on the presence or absence of the pyroelectric, it causes a decrease in the temperature amplitude limit.

Figure 9 Impact of control gain $G = 1 \times 10^6$ on non-dimensionalised dynamic temperature of the plate and pyroelectric effect is not included
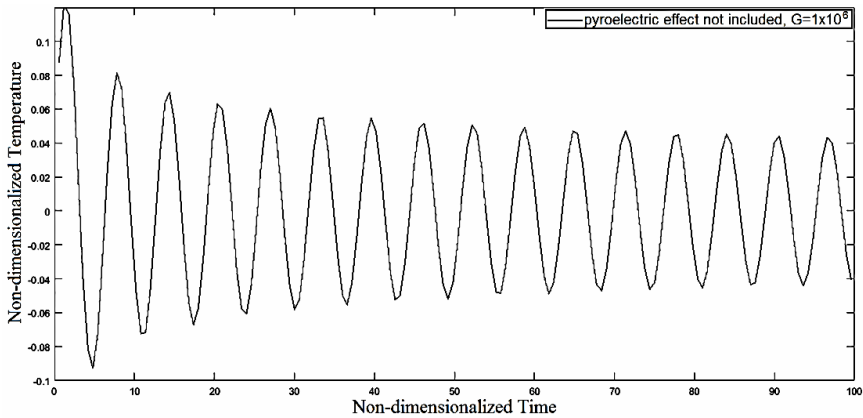
Figure 10 Impact of control gain $G = 1 \times 10^6$ on non-dimensionalised dynamic temperature of the plate and pyroelectric impact is included
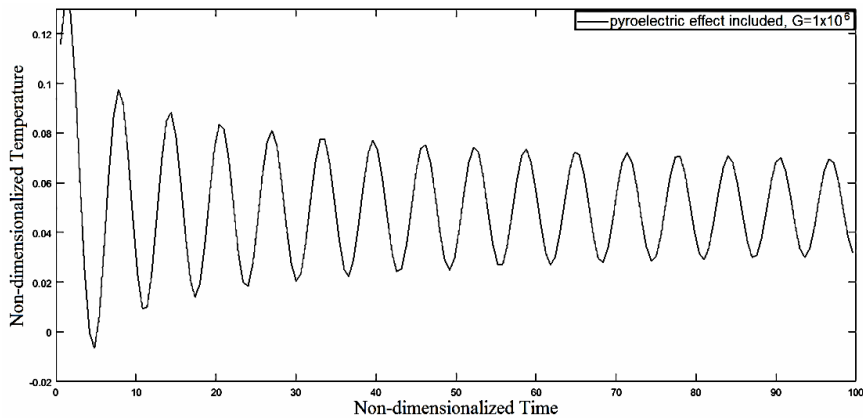
The investigation on the control behaviour of smart composite plates includes the piezoelectric control gain effect on the temperature and deflection magnitudes. Another goal of the current study is to examine the corresponding temperature response on the behaviour of active laminated composite plates exposed subjected to the hygrothermal environment regarding the pyroelectric impacts. Figures 9 and 11 demonstrate the impact of different control gains on the plate's temperature minus the pyroelectric impact. As it

is obvious by applying the control gain, the temperature initially increased, then it has been eventually damped. Figures 10 and 12 indicate the impact of different control gains on the temperature of the plate regarding the pyroelectric impact. By comparing Figures 9 and 11 with Figures 10 and 12, respectively, it can be understood that by considering the pyroelectric impact, the plate temperature amplitude will be drastically decreased.

Figure 11   Impact of control gain $G = 2 \times 10^6$ on non-dimensionalised dynamic temperature of the plate and pyroelectric impact is not included
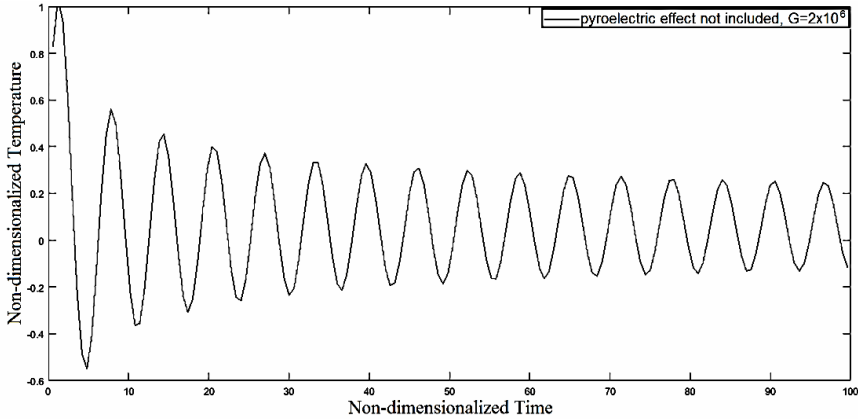
Figure 12   Impact of control gain $G = 2 \times 10^6$ on non-dimensionalised dynamic temperature of the plate and pyroelectric impact is included
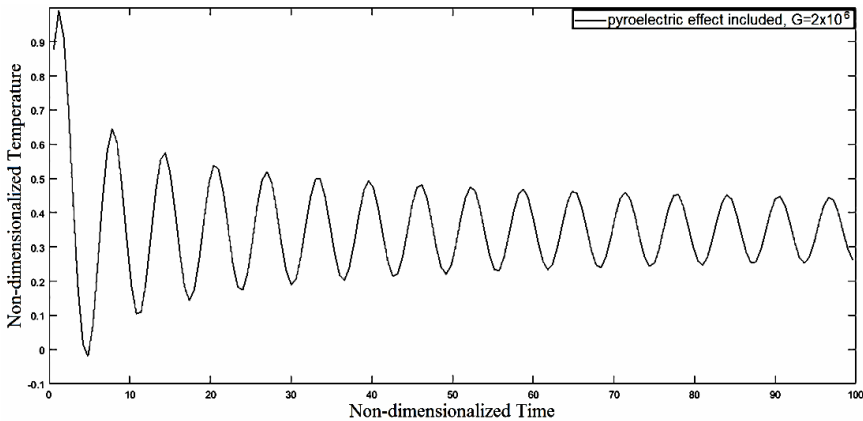
Figure 13 corresponds to the control gain influence on the central deflection's dynamic response. The results clearly show that by increasing moisture diffusion, the number of stresses and deflection are increased, and because of that, the temperature is also increased. It is also shown that by applying appropriate control gain to the actuator layer, the deflection of the plate can be controlled and damped entirely. The control gains rise can propose greater vibration amplitude with a more accelerated rate of amplitude suppression. That is a substantial consideration for accuracy sensing and control.

Figure 13 Control gains impact G = 1 × 10⁶ and G = 4 × 10⁶ on non-dimensionalised dynamic response of the central deflection
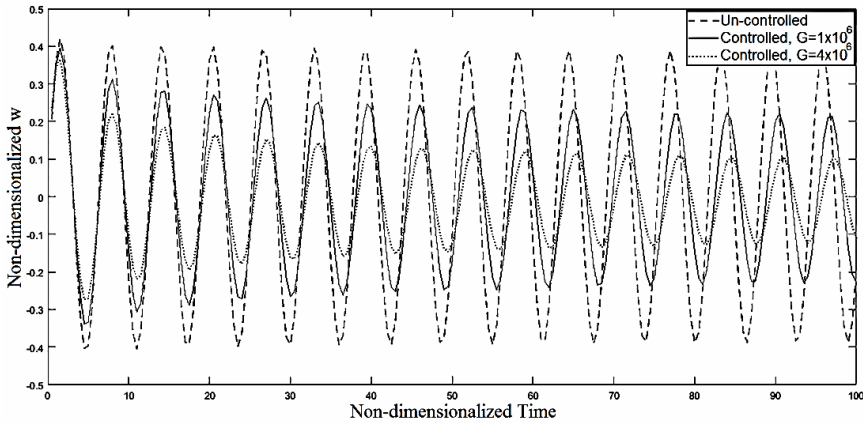
4 Conclusions

This paper is mainly focused on analysing the hygrothermal impact over the coupled thermopiezoelastic composite plates. The dynamic deflection and stresses of a coupled thermo-piezo-elastic rectangular composite plate stemmed from quickly applied mechanical excitations derived from considering heat equation, under hygrothermal environment. The temperature hypothetical linear distribution equation through the thickness is considered to show the temperature of any point of the plate, which is solved as a coupling with other equations. Thermoelastic and pyroelectric effects are part of the constitutive equations.

The results show that by increasing moisture diffusion, the number of stresses and deflections are increased, and consequently, the induced temperature is increased as by increasing humidity up to 25%. A change of 5% deflection rise and on average 4% increase of stresses are observed. Furthermore, if the increase of humidity goes to 75% the plate deflection grows by 9% and stresses increase about 8%, where the σ_{xy} has fewer effective stresses against σ_x and σ_y. It is also noticeable that by applying appropriate control gain to the actuator layer, the deflection of the plate can be controlled and damped entirely. However, it is evident that the control gain can change the temperature and deflection. As clearly shown in the paper, by using control gain G = 1 × 10⁶, the deflection damped 38% faster and when it is increased to G = 4 × 10⁶, the deflection damped 62% quicker which causes the heat generated in the plate controlled properly. It can also be seen that the pyroelectric has not a major effect on transverse deflection however its impact on the temperature amplitude of the plate is significant. When laminated plate is exposed to a more significant temperature or under humid circumstances, stresses are developed. Regarding temperature and moisture factors involved simultaneously, the growth rate of stresses and deflection reaches its maximum value.

This work can be extended to add some tests including buckling, fatigue, ductility and toughness. In the future, the authors plan to investigate the effect of the same conditions presented in the paper for strains and elastic behaviour and use different theories to solve the existing equations to compare the accuracy of the results.

References

Babaei, M.H., Abbasi, M. and Eslami, M.R. (2018) 'Coupled thermoelasticity of functionally graded beams', *Journal of Thermal Stresses*, Vol. 31, No. 8, pp.680–697.

Benkhedda, A. and Tounsi, A. (2008) 'Effect of temperature and humidity on transient hygrothermal stresses during moisture desorption in laminated composite plates', *Composite Structures*, Vol. 82, No. 4, pp.629–635.

Brischetto, S. and Carrera, E. (2018) 'Thermal stress analysis by refined multilayered composite shell theories', *Journal of Thermal Stresses*, Vol. 32, No. 1, pp.165–186.

Brunner, A.J., Hack, E. and Neuenschwander, J. (2015) *Encyclopedia of Polymer Science and Technology*, John Wiley & Sons, New York.

Carrera, E., Cinefra, M. and Fazzolari, F.A. (2013) 'Some results on thermal stress of layered plates and shells by using unified formulation', *Journal of Thermal Stresses*, Vol. 36, No. 6, pp.589–625.

Cho, K.N., Striz, A.G. and Bert, C.W. (2007) 'Thermal stress analysis of laminate using higher-order theory in each layer', *Journal of Thermal Stresses*, Vol. 12, No. 3, pp.321–332.

Cinefra, M., Petrolo, M., Li, G. and Carrera, E. (2017) 'Hygrothermal analysis of multilayered composite plates by variable kinematic finite elements', *Journal of Thermal Stresses*, Vol. 40, No. 12, pp.1502–1522.

Eslami, M.R., Hetnarski, R.B., Ignaczak, J., Noda, N., Sumi, N. and Tanigawa, Y. (2013) *Theory of Elasticity and Thermal Stresses*, Springer, Berlin.

Eslami, M.R., Shakeri, M., Ohadi, A.R. and Shiari, B. (1999) 'Coupled thermoelasticity of shells of revolution: effect of normal stress and coupling', *AIAA Journal*, Vol. 37, No. 4, pp.496–504.

Haghgoo, M., Ansari, R., Hassanzadeh-Aghdam, M.K. and Darvizeh, A. (2019) 'Fully coupled thermo-magneto-electro-elastic properties of unidirectional smart composites with a piezoelectric interphase', *Proceedings of the Institution of Mechanical Engineers, Part C: Journal of Mechanical Engineering Science*, Vol. 233, No. 8, pp.2813–2829.

Heidary, F. and Eslami, M.R. (2004) 'Dynamic analysis of distributed piezothermoelastic composite plate using first-order shear deformation theory', *Journal of Thermal Stresses*, Vol. 27, No. 7, pp.587–605.

Heidary, F. and Eslami, M.R. (2005) 'Pyroelectric effect on dynamic response of coupled distributed piezothermoelastic composite plate', *Journal of Thermal Stresses*, Vol. 28, No. 3, pp.285–300.

Heidary, F. and Eslami, M.R. (2016) 'Piezo-control of forced vibrations of a thermoelastic composite plate', *Composite Structures*, Vol. 74, No. 1, pp.99–105.

Hwu, C., Hsu, H.W. and Lin, Y.H. (2017) 'Free vibration of composite sandwich plates and cylindrical shells', *Composite Structures*, Vol. 2017, No. 171, pp.528–537.

Lam, K.Y., Peng, X.Q., Liu, G.R. and Reddy, J.N. (1997) 'A finite-element model for piezoelectric composite laminates', *Smart Materials and Structures*, Vol. 6, No. 5, pp.583–591.

Liew, K.M., Zhang, J.Z., Li, C. and Meguid, S.A. (2015) 'Three-dimensional analysis of the coupled thermo-piezoelectro-mechanical behaviour of multilayered plates using the differential quadrature technique', *International Journal of Solids and Structures*, Vol. 42, No. 14, pp.4239–4257.

Liu, C., Bian, Z., Chen, W. and Lü, C. (2012) 'Three-dimensional pyroelectric analysis of a functionally graded piezoelectric hollow sphere', *Journal of Thermal Stresses*, Vol. 35, No. 6, pp.499–516.

Lo, S.H., Zhen, W., Cheung, Y.K. and Wanji, C. (2020) 'Hygrothermal effects on multilayered composite plates using a refined higher order theory', *Composite Structures*, Vol. 92, No. 3, pp.633–646.

Phung-Van, P., De Lorenzis, L., Thai, C.H., Abdel-Wahab, M. and Nguyen-Xuan, H. (2015) 'Analysis of laminated composite plates integrated with piezoelectric sensors and actuators using higher-order shear deformation theory and isogeometric finite elements', *Computational Materials Science*, Vol. 2015, No. 96, pp.495–505.

Ray, M.C., Bhattacharya, R. and Samanta, B. (2019) 'Exact solutions for static analysis of intelligent structures', *AIAA Journal*, Vol. 31, No. 9, pp.1684–1691.

Reddy, J.N. (2006) *Theory and Analysis of Elastic Plates and Shells*, CRC Press, Boca Raton.

Robaldo, A. and Carrera, E. (2007) 'Mixed finite elements for thermoelastic analysis of multilayered anisotropic plates', *Journal of Thermal Stresses*, Vol. 30, No. 2, pp.165–194.

Sereir, Z., Adda-Bedia, E. and Tounsi, A. (2015) 'Effects of the accelerated moisture diffusivity on the hygrothermal behavior on a laminated plate with symmetrical environmental conditions', *Journal of Thermal Stresses*, Vol. 28, No. 9, pp.889–910.

Sereir, Z., Adda-Bedia, E.A. and Tounsi, A. (2006) 'Effect of temperature on the hygrothermal behaviour of unidirectional laminated plates with asymmetrical environmental conditions', *Composite Structures*, Vol. 72, No. 3, pp.383–392.

Sousa, C.S., Camanho, P.P. and Suleman, A. (2013) 'Analysis of multistable variable stiffness composite plates', *Composite Structures*, Vol. 2013, No. 98, pp.34–46.

Wang, X., Dong, K. and Wang, X.Y. (2010) 'Hygrothermal effect on dynamic interlaminar stresses in laminated plates with piezoelectric actuators', *Composite Structures*, Vol. 71, No. 2, pp.220–228.